

Article

The Influence of Oxygen Concentration during MAX Phases (Ti_3AlC_2) Preparation on the $\alpha\text{-Al}_2\text{O}_3$ Microparticles Content and Specific Surface Area of Multilayered MXenes ($\text{Ti}_3\text{C}_2\text{T}_x$)

Błażej Scheibe ^{1,*}, Wojtech Kupka ², Barbara Peplińska ¹, Marcin Jarek ¹ and Krzysztof Tadyszak ¹

¹ NanoBioMedical Centre, Adam Mickiewicz University, 61 614 Poznań, Poland; barbara.peplinska@amu.edu.pl (B.P.); marcin.j@amu.edu.pl (M.J.); tadyszak@amu.edu.pl (K.T.)

² Regional Centre for Advanced Technologies and Materials, Department of Physical Chemistry, Faculty of Science, Palacky University Olomouc, 771 46 Olomouc, Czech Republic; wojtech.kupka@gmail.com

* Correspondence: bscheibe@amu.edu.pl

Received: 30 November 2018; Accepted: 6 January 2019; Published: 23 January 2019



Abstract: The high specific surface area of multilayered two-dimensional carbides called MXenes, is a critical feature for their use in energy storage systems, especially supercapacitors. Therefore, the possibility of controlling this parameter is highly desired. This work presents the results of the influence of oxygen concentration during Ti_3AlC_2 ternary carbide—MAX phase preparation on $\alpha\text{-Al}_2\text{O}_3$ particles content, and thus the porosity and specific surface area of the $\text{Ti}_3\text{C}_2\text{T}_x$ MXenes. In this research, three different Ti_3AlC_2 samples were prepared, based on TiC-Ti₂AlC powder mixtures, which were conditioned and cold pressed in argon, air and oxygen filled glove-boxes. As-prepared pellets were sintered, ground, sieved and etched using hydrofluoric acid. The MAX phase and MXene samples were analyzed using scanning electron microscopy and X-ray diffraction. The influence of the oxygen concentration on the MXene structures was confirmed by Brunauer-Emmett-Teller surface area determination. It was found that oxygen concentration plays an important role in the formation of $\alpha\text{-Al}_2\text{O}_3$ inclusions between MAX phase layers. The mortar grinding of the MAX phase powder and subsequent MXene fabrication process released the $\alpha\text{-Al}_2\text{O}_3$ impurities, which led to the formation of the porous MXene structures. However, some non-porous $\alpha\text{-Al}_2\text{O}_3$ particles remained inside the MXene structures. Those particles were found ingrown and irremovable, and thus decreased the MXene specific surface area.

Keywords: MAX phases; Ti_3AlC_2 ; MXenes; $\text{Ti}_3\text{C}_2\text{T}_x$; $\alpha\text{-Al}_2\text{O}_3$ particles; porosity

1. Introduction

Since the discovery of graphene [1], the scientific trend in nanomaterial sciences turned toward two-dimensional (2D) nanostructures. One of the most intensively investigated groups of 2D nanostructures are transition metal carbides, nitrides and carbonitrides called MXenes [2,3]. MXenes are derived from MAX phases, layered and hexagonal nanolaminates named for their general formula— $\text{M}_{n+1}\text{AX}_n$. The M is a transition metal, the A is an A group (mostly IIIA and IVA) element and the X is a C and/or N. The n parameter ($n = 1, 2$ or 3) determines the formation of the 211, 312 or 413 structures [4]. The removal of the A layer via wet chemistry methods leads to the formation of MXenes ($\text{M}_{n+1}\text{X}_n\text{T}_x$)—multilayered accordion-like structures, where T_x refers to Ti-bonded -F, -OH or -O functional groups [5]. The first obtained MXene was $\text{Ti}_3\text{C}_2\text{T}_x$, derived from a Ti_3AlC_2 MAX

phase via Al layer removal [6]. Later, the delamination of $\text{Ti}_3\text{C}_2\text{T}_x$ toward single-layers led to an increase in the specific surface area (SSA) and allowed for one of the highest volumetric capacitances (520 F/cm^3 at 2 mV/s), which exposed them as a potential candidate for electrical double layer capacitors [7]. Thanks to their lamellar structure, conductive core and hydrophilic surface, MXenes can host many different cations between their layers. Thus, they can be widely applied in different energy storage devices, such as in Na-ions [8] and Li-S batteries [9], supercapacitors [10] or other branches of science like adsorption [11] and catalysis [12]. Currently, the SSA of the multilayered MXenes is controlled at the post-formation stage via different approaches: (i) increasing the distance between layers via intercalation with ions or guest molecules [13], (ii) physical adsorption or covalent linkage with guest molecules or nanoparticles [14], and (iii) formation of composites with other 2D nanomaterials [15]. In our work we took a totally different approach and investigated the possibility of controlling the porosity and specific surface area of multilayered $\text{Ti}_3\text{C}_2\text{T}_x$ MXenes at the pre-formation stage—during the preparation of the Ti_3AlC_2 MAX phase. The accordion-like MXene structure is held together by hydrogen bonds between functional groups of individual graphene-like MXene sheets [16]. However, our observations indicated that the multilayered structures are also stable due to presence of the $\alpha\text{-Al}_2\text{O}_3$ particles ingrown inside MXene microparticles. We deduced that the $\alpha\text{-Al}_2\text{O}_3$ particles are formed during MAX phase sintering, depending on the oxygen concentration. This process is similar to the formation of TiC impurities in the MAX phase matrix, where the non-stoichiometric composition of the starting powders leads to the occurrence of carbon excess or aluminum deficiency during the sintering of the Ti-Al-C based MAX phases [17]. In order to prove our hypothesis, we prepared three different Ti_3AlC_2 samples, where TiC- Ti_2AlC powder mixtures were conditioned and cold pressed into pellets in argon, air and oxygen environments. Both Ti_3AlC_2 and $\text{Ti}_3\text{C}_2\text{T}_x$ samples were investigated by means of scanning electron microscopy (SEM), X-ray diffraction (XRD) and physisorption analyses. As expected, the environmental oxygen concentration during MAX phase preparation had a significant influence on the amount of Al_2O_3 impurities in different MXene samples, and thus on their porosity and specific surface area.

2. Materials and Methods

2.1. Materials

All the reagents were of analytical grade and used without further purification. Absolute ethanol (99.8%) was purchased from POCH. Hydrofluoric acid (HF) (48%), phosphoric acid ($\geq 99\%$) and titanium carbide (98%) (325 mesh) were obtained from Sigma-Aldrich. Maxthal 211— Ti_2AlC (325 mesh) was purchased from Kanthal (Hallsthammar, Sweden). The N_2 (5.0), Ar (5.0) and O_2 (5.0) were purchased from Linde (Kraków, Poland). All solutions were prepared on the basis of MilliQ ($13.6 \text{ M}\Omega/\text{cm}$) type 1 water ($\text{T1-H}_2\text{O}$).

2.2. MAX Phase and MXene Synthesis

The MXene samples were obtained from Ti_3AlC_2 MAX sinters prepared under different conditions. Briefly, three mixtures of Ti_2AlC and TiC powders (1:1 molar ratio) were weighed in air and mixed by ball milling in air for 12 h (agate grinding jars and balls). Each powder mixture was conditioned in a glove-box for 24 h in a different gas environment: (1) argon, (2) air or (3) oxygen, and subsequently cold pressed (10 tons) into 13 mm pellets inside the glove-box. The as-prepared pellets were transferred from the glovebox to a horizontal tube furnace. Ti_3AlC_2 MAX phases were prepared via the volume combustion synthesis of pellets at $1350 \text{ }^\circ\text{C}$ (ramp $10 \text{ }^\circ\text{C}/\text{min}$) in Ar flow for 2 h. The pellets were ground in 99.5% alumina mortar and sieved through a 400 mesh sieve. As-prepared Ti_3AlC_2 microparticle powders ($< 37 \text{ }\mu\text{m}$) were labeled $\text{Ti}_3\text{AlC}_2\text{-Ar}$, $\text{Ti}_3\text{AlC}_2\text{-Air}$ and $\text{Ti}_3\text{AlC}_2\text{-O}_2$ according to the preparation conditions. Three MAX phase powders underwent aluminum layer etching with hydrofluoric acid (2 g $\text{Ti}_3\text{AlC}_2/20 \text{ mL HF}$) in plastic jars at $40 \text{ }^\circ\text{C}$ for 24 h under continuous stirring. As-obtained $\text{Ti}_3\text{C}_2\text{T}_x\text{-Ar}$, $\text{Ti}_3\text{C}_2\text{T}_x\text{-Air}$ and $\text{Ti}_3\text{C}_2\text{T}_x\text{-O}_2$ microparticles were purified through cycles of washing with

Ti-H₂O and centrifugation 24,000 rpm for 5 min, until the supernatant reached a pH of 6.5. All purified samples were dispersed in absolute ethanol and left overnight on a Petri dish to evaporate in the oven at 80 °C for further characterization.

2.3. Characterization

The MAX phase and MXene samples morphology was investigated by scanning electron microscopy (SEM) (JEM-7001TTLS, JEOL, Akishima, Japan). Powder X-ray diffraction (XRD) studies of Ti₃AlC₂ and Ti₃C₂T_x were carried out on an Empyrean (PANalytical, Royston, UK) diffractometer using Cu K α radiation (1.54 Å), reflection-transmission spinner (sample stage) and PIXcel3D detector. Surface area and pore size analyses of MXenes and MAX powders were performed by means of N₂ adsorption-desorption measurements at −196.15 °C on a volumetric gas adsorption analyzer (3Flex, Micromeritics, Norcross, GA, USA) up to 0.965 P/P₀. Prior to the analysis, the samples were degassed in a vacuum (7 × 10^{−2} mbar) for 12 h at 130 °C, while high purity (99.999%) N₂ and He gases were used for the measurements. The Brunauer-Emmett-Teller area (BET) was determined with respect to Rouquerol criteria for BET determination in the range of 0.1–0.3 P/P₀, assuming a molecular cross-sectional area of 16.2 Å² for N₂. The isotherms were further analyzed for pore size calculation using the Barret-Joyner-Halenda (BJH) method. An average slit-pore width was calculated according to the formula:

$$\overline{w}_p = 2V/S_{BET} \quad (1)$$

where \overline{w}_p is an average slit-pore width, V is the total pore volume and S_{BET} is the surface area [18].

3. Results and Discussion

X-ray diffraction is an essential technique proving the successful synthesis of Ti₃AlC₂ MAX phases and the formation of Ti₃C₂T_x MXenes. Figure 1 presents XRD patterns of powder precursors (TiC/Ti₂AlC) (Figure 1A) and all prepared samples (Ti₃AlC₂/Ti₃C₂T_x) (Figure 1B–D). The TiC XRD pattern exhibits five diffraction peaks at $2\theta = 35.9^\circ$ (111), 41.73° (200), 60.44° (220), 72.34° (311) and 76.11° (222), which correspond to pure face-centered cubic TiC phase [19]. The commercial Ti₂AlC powder exhibits nine 211 MAX phase specific peaks at $2\theta = 12.95^\circ$ (002), 26.08° (004), 33.80° (100), 39.52° (103), 43.17° (104), 52.97° (106), 60.53° (110), 71.55° (109) and 74.61° (116). The highly intense (002) peak indicates a high degree of crystallinity of the material. The Ti₂AlC powder is contaminated to some extent with Ti₃AlC₂, TiC and γ -Ti₂Al₅ particles, which presence is confirmed in the XRD spectrum [20]. Regardless of the environment in which TiC and Ti₂AlC powder mixtures were conditioned and cold pressed, the sintering of pellets led to the formation of the Ti₃AlC₂. All Ti₃AlC₂ samples presented similar XRD patterns and shown fourteen 312 MAX phase peaks at $2\theta = 9.57^\circ$ (002), 19.2° (004), 34.05° (101), 36.79° (103), 39.05° (104), 41.86° (105), 44.99° (106), 48.55° (107), 54.34° (108), 56.57° (109), 60.45° (110), 65.64° (1011), 70.57° (2021) and 74.14° (2024) [21]. The position of the peaks was almost identical with non-significant shifts. The only difference was observed in the intensities of the (002), (004) and (103) peaks. No peaks related to the 211 Ti₂AlC phase were observed. However, the Ti₃AlC₂ XRD patterns exhibited five TiC-related peaks: (111), (200), (220), (311), (222) as well as eight peaks at $2\theta = 25.56^\circ$ (012), 35.14° (104), 37.76° (110), 43.33° (113), 52.53° (024), 57.48° (116), 66.50° (214) and 68.19° (300), which corresponded to the α -Al₂O₃ particles [22]. The removal of the Al layer from the MAX phases led to disappearance of all the Ti₃AlC₂ related peaks and shift of the (002) and (004) peaks toward lower values from $2\theta = 9.57^\circ$ and 19.19° to $2\theta = 8.86^\circ$ and 18.04° , respectively. In general, the shift and broadening of the (002) peak indicated the successful formation of the MXenes [23]. The Ti₃C₂T_x XRD patterns also exhibited peaks related to TiC and α -Al₂O₃, both of which are well known contaminants of multilayered MXene structures [24]. The TiC and α -Al₂O₃ particles were formed during the Ti₃AlC₂ sintering and remained as impurities after Al removal [25]. Interestingly, the TiC and α -Al₂O₃ related peaks became sharper and their intensities increased after aluminum etching. The highest increase was observed for the Ti₃C₂T_x-O₂ and it was not related to the

preferred orientation of the MXene powder on the Si holder but rather to oxygen availability during the sintering. This observation could be explained by the following:

- (1) increased O_2 concentration led to increased formation of Al_2O_3 ;
- (2) increased Al_2O_3 formation led to a decreased availability of Al atoms for Ti_3AlC_2 synthesis;
- (3) decreased Al atoms content led to increased formation of TiC due to stoichiometry disturbance.

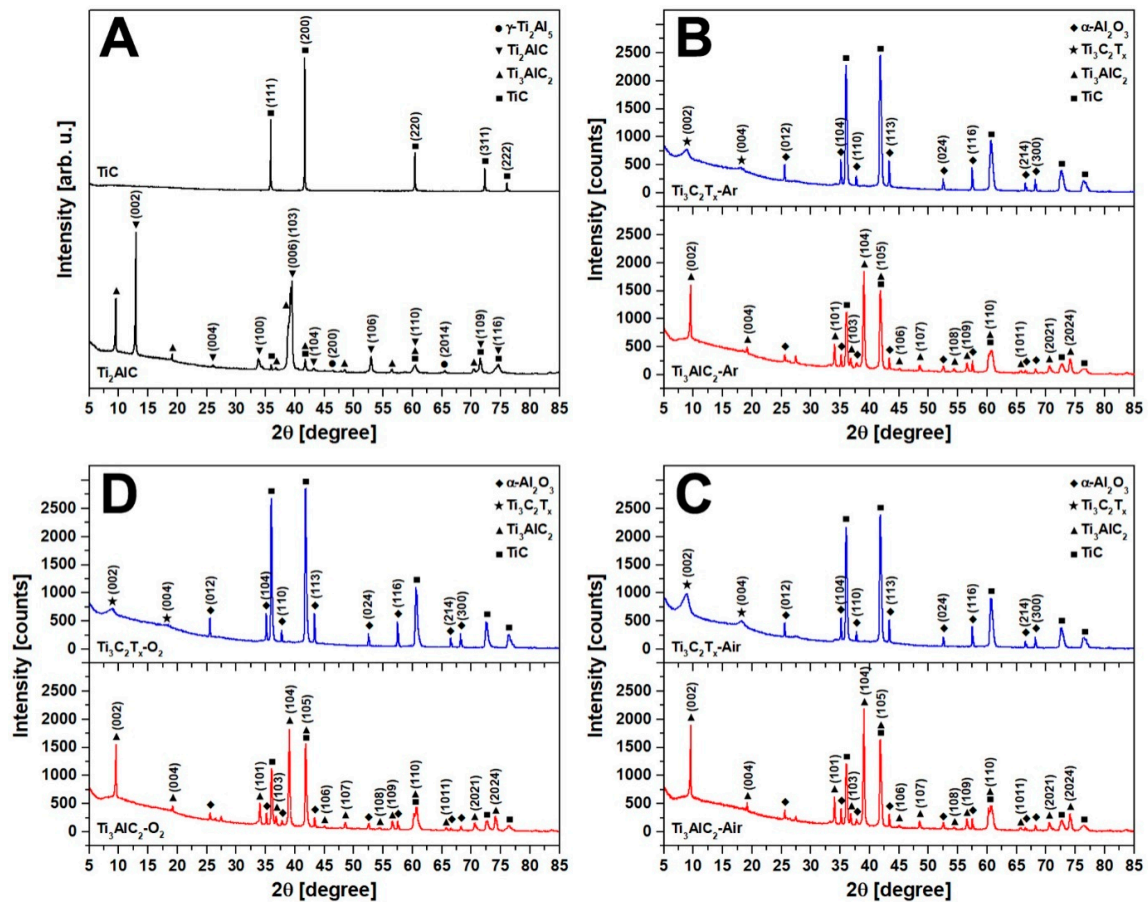


Figure 1. The XRD patterns of (A) TiC/ Ti_2AlC powders as well as Ti_3AlC_2 / $Ti_3C_2T_x$ obtained by powder mixtures prepared in (B) argon, (C) air and (D) oxygen environments.

The morphologies of the Ti_3AlC_2 and $Ti_3C_2T_x$ samples prepared in different environments are shown in Figure 2. All presented micrographs are representative of the majority of each sample. The top, middle and bottom rows correspond to: (i) lightly ground MAX phase pellets (Figure 2A–C), (ii) sieved MAX phase powders (Figure 2D–F), and (iii) purified MXene powders (Figure 2G–I), respectively. The left, middle and right columns are related to the samples prepared by powder mixtures conditioned in Ar, air and O_2 environments, respectively. From Figure 2A–C one can see that regardless of the applied gas, MAX phase pellets possessed a layered structure. The only difference was the amount of nonconductive $\alpha-Al_2O_3$ particles (shining white due to charge accumulation) or the number of holes after they fell out. All investigated samples were contaminated with alumina particles, which is in agreement with the XRD analyses. The morphology of Ti_3AlC_2 -Ar and Ti_3AlC_2 -Air was similar. The $\alpha-Al_2O_3$ particles presence in the Ti_3AlC_2 -Ar samples was unexpected. At first we suspected oxygen molecules adsorbed onto the cold-pressed pellet's surface during its exposition to environmental air while being transferred from the glovebox to the horizontal furnace. The evaporating Al in contact with adsorbed O_2 molecules formed an Al_2O_3 layer on sintered pellet surface. However, the morphology is quite different because the Al_2O_3 layer is made of particles in the

form of rods and needles (Figure S1). Therefore, we believe that the formation of α -Al₂O₃ particles in the Ti₃AlC₂ matrix was caused by the availability of atmospheric oxygen during the weighing and mixing of the powders. The 24 h conditioning of the powder mixture in Ar did not lead to desorption of the O₂ molecules. Aluminum has a high affinity to O₂ so in order to prepare perfect Ti₃AlC₂ MAX phases, all preparation steps should be performed in an Ar filled glovebox [26].

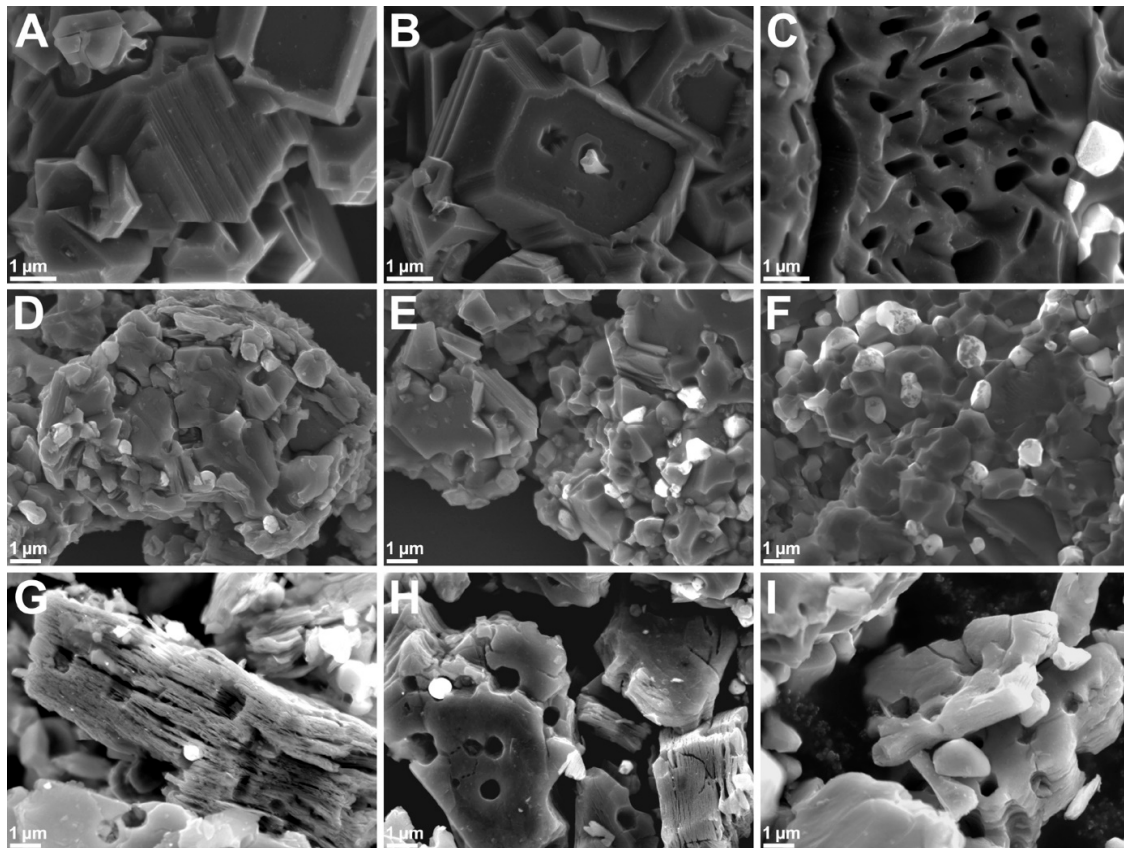


Figure 2. SEM micrographs of MAX phase pellets (A–C), ground powders (D–F) and purified MXene particles (G–I) prepared in Ar (A,D,G), Air (B,E,H) and O₂ (C,F,I) environments.

In the case of Ti₃AlC₂-O₂ (Figure 2F) one can observe a plethora of alumina particles. Both α -Al₂O₃ and holes from which the particles fell are present in the derived multilayered MXenes (Figure 2G–I). We tried to remove α -Al₂O₃ particles using H₃PO₄ solutions in a concentration range of 5% to 95%, as well as etchant mixtures for the removal of thin layers of Al₂O₃, but without success. Then, we tried to remove α -Al₂O₃ mechanically by stirring, shaking, sieving and exploiting the difference in solubility via multiple cycles of dispersing/centrifugation, but with little success. We performed comprehensive SEM analyses of MXene structures comparing micrographs captured in classic SEI (secondary electron imaging) and COMPO (backscattering electrons) modes as well as with EDS mapping and elemental analysis (Figure 3). The application of COMPO mode (Figure 3B) allowed us to distinguish the lighter and heavier atoms in the SEM image. Lighter elements appeared darker, while heavier appeared lighter. This mode was used to distinguish MXene structures from α -Al₂O₃ particles and to reveal the position of alumina particles in the structure. Comparing Figure 3A,B, one can see the alumina particles that are hidden in the MXene structure beneath the top Ti₃C₂T_x layers. This observation proves that they were formed during Ti₃AlC₂ sintering and were not introduced to the MAX phase structure by powder grinding in alumina mortar or from the remains of the Al₂O₃ layer that was mechanically removed from Ti₃AlC₂ pellet surface. The presence of α -Al₂O₃ particles was also confirmed by EDS mapping and analyses performed on top of the microparticle and MXene (Figure 3C). The Al and O distribution maps clearly describe the α -Al₂O₃ position in the MXene sample. Spectrum 1 of the

α -Al₂O₃ exhibited intense Al (18.83% atomic—at.) and O (59.03% at.) peaks at $K\alpha = 1.486$ keV and $K\alpha = 0.525$ keV, respectively. The intensities of the peaks related to Ti (3.35% at.), C (14.70% at.) and F (4.09% at.) at $K\alpha = 4.508/L\alpha = 0.452$ keV, $K\alpha = 0.277$ keV and $K\alpha = 0.677$ keV, respectively, were low and could be assigned to some MXene fragments remaining on the α -Al₂O₃ surface. In the case of Spectrum 2, the intensities of Al (1.78% at.) and O (18.21% at.) peaks were low, while MXene peaks: Ti (20.12% at.), C (27.69% at.) and F (32.20% at.) dominated. The presence of O atoms confirmed the existence of the MXene terminal groups, while the Al presence could have been related to the surface adsorbed AlF₃ impurities. Profound SEM analysis of the Ti₃C₂T_x-Air sample revealed that α -Al₂O₃ particles were not only hidden in the MXene structure but were grown in and covered by MXenes (Figure 3D,E), proving again that they were formed during MAX phase sintering. This is the reason why α -Al₂O₃ impurities are so hard to remove and why it is important to control the oxygen concentration during MAX phase preparation. This led us to conclude that multilayered MXenes are not only held together by the hydrogen bonds between Ti₃C₂T_x monolayers, but also grown in α -Al₂O₃ particles. The majority of the alumina particles possessed a spherical shape. However, some of them grew in a triangular or tooth-like shape (Figure S2). This observation indicates that the α -Al₂O₃ impurities formed during MAX phase sintering adopted their shape to the limited space available between the forming Ti₃AlC₂ layers.

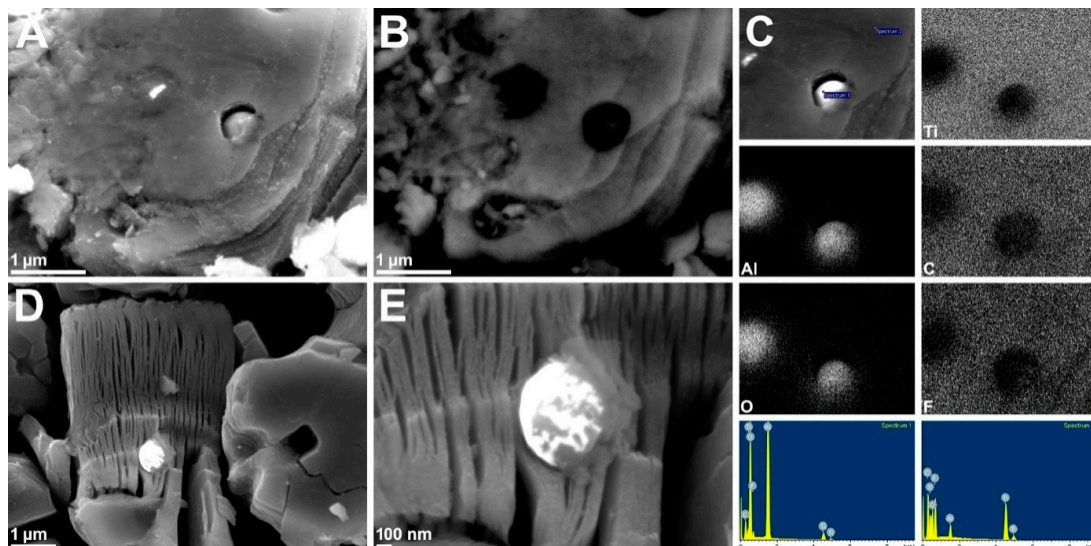


Figure 3. SEM micrographs of Ti₃C₂T_x-Air in SEI (A,D,E), COMPO (B) modes, and EDS analyses (C).

The specific surface area, pore volume and pore size distribution of the MAX phases and derived MXenes were determined from physisorption measurements. The N₂ adsorption isotherms are shown in Figure 4.

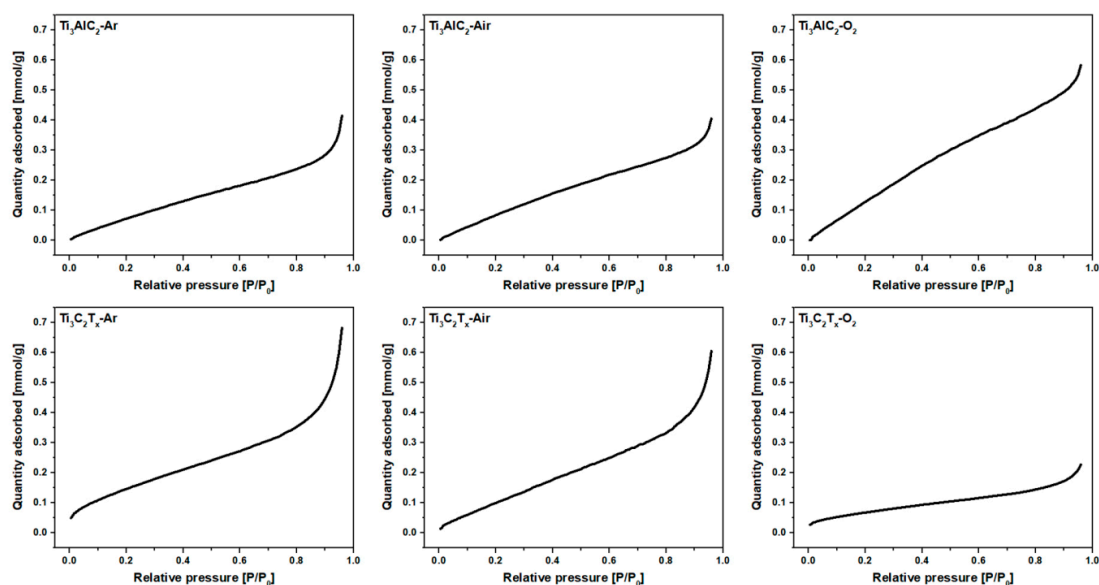


Figure 4. The N_2 adsorption isotherms of MAX phase and MXene powders.

According to International Union of Pure and Applied Chemistry (IUPAC) classification, all isotherms corresponded to the Type II isotherm, which is typical for macroporous solids [27]. The calculated specific surface area, pore volume and pore diameters are presented in Table 1.

Table 1. Specific surface area, pore volume and pore diameters calculated for investigated MAX phases and derived MXenes.

Sample	Specific Surface Area (m^2/g)	Pore Volume (cm^3/g)	Average Pore Width (BJH) (nm)	Average Slit-Pore Width (nm)
Ti_3AlC_2 -Ar	10.57	0.0133	6.58	2.5
Ti_3AlC_2 -Air	12.95	0.0134	5.51	2.1
Ti_3AlC_2 - O_2	22.46	0.0195	5.12	1.7
$Ti_3C_2T_x$ -Ar	13.70	0.0219	6.86	3.2
$Ti_3C_2T_x$ -Air	13.64	0.0196	6.30	2.9
$Ti_3C_2T_x$ - O_2	5.96	0.0075	5.38	2.5

In the case of MAX phase powders, the Ti_3AlC_2 -Ar and Ti_3AlC_2 - O_2 samples shown the highest and the lowest SSA, respectively. This effect is related to the concentration of holes remaining in the Ti_3AlC_2 structure after mechanical removal of the α - Al_2O_3 particles during the grinding process, what was previously observed in SEM micrographs (Figure 2A,C). According to the different scientific reports, the SSA of multilayered $Ti_3C_2T_x$ is in the range of 5 to 90 m^2/g , which is related to the (i) preparation method [28], (ii) state of oxidation/decomposition [29], and (iii) intercalated ions or guest molecules [30–32]. The SSA values of the investigated samples were typical for multilayered MXenes. For the $Ti_3C_2T_x$ -Ar and $Ti_3C_2T_x$ -Air samples, the SSA values were higher in comparison with the parental MAX phases, which was due to the removal of the Al atoms after HF etching. All the MXene samples were contaminated by various amounts of TiC and α - Al_2O_3 impurities. Based on the XRD and SEM analyses, the highest concentration of non-porous particles was expected for the $Ti_3C_2T_x$ - O_2 sample. This assumption was fully confirmed by the two-fold lower SSA value compared with the other investigated MXene samples, and by almost a three-fold lower pore volume in comparison with $Ti_3C_2T_x$ -Ar. The physisorption measurements of the MAX phase and MXene powders clearly shown the influence of high oxygen concentration, during pellet preparation, on the formation of non-porous impurities in MAX phases, and thus MXenes porosity. Based on the information obtained through XRD analyses, SEM-EDS investigations and physisorption measurements, the formation of α - Al_2O_3

particles in the Ti_3AlC_2 matrix as well as their fate after conversion of the MAX phases to MXene structures is presented schematically in Figure 5.

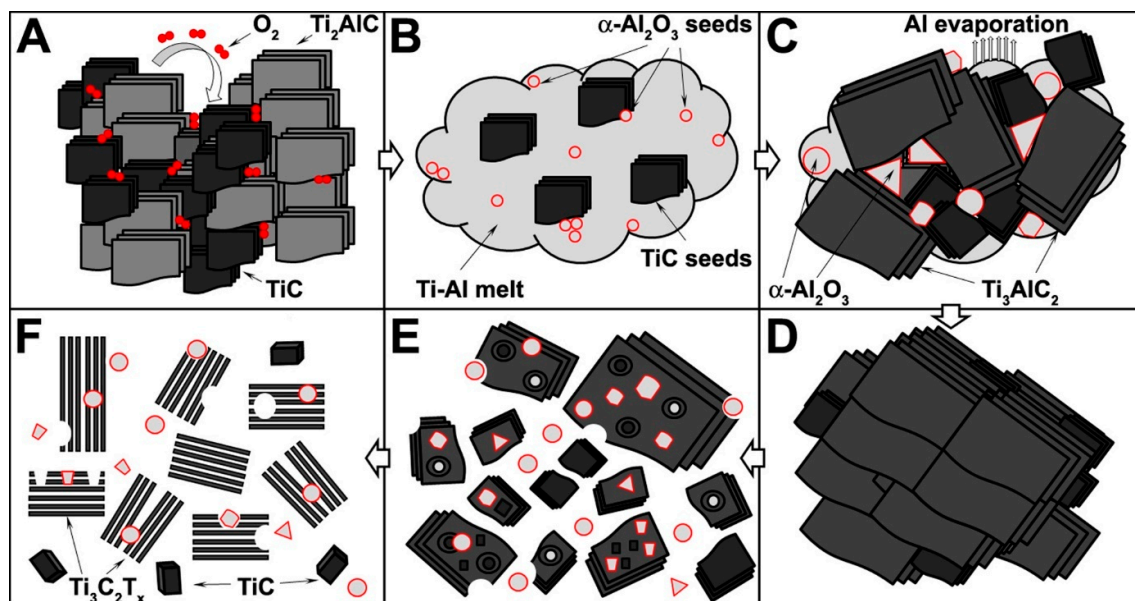


Figure 5. The formation of $\alpha\text{-Al}_2\text{O}_3$ microparticles during Ti_3AlC_2 MAX phase synthesis.

At first, the oxygen molecules are adsorb on the $\text{TiC}/\text{Ti}_2\text{AlC}$ particle surface and remain there during pellet preparation (Figure 5A). Next, Ti-Al melt forms at the early stages of the sintering process. The adsorbed O_2 molecules form the initial $\alpha\text{-Al}_2\text{O}_3$ seeds with Al atoms released from the Ti_2AlC MAX phase. The decomposition of Ti_2AlC also leads to the formation of TiC grains (Figure 5B). When the temperature reaches $1350\text{ }^\circ\text{C}$, the following events occur: (i) Ti_3AlC_2 layers start to precipitate from Ti-Al melt, (ii) the Al atoms evaporate, (iii) the $\alpha\text{-Al}_2\text{O}_3$ grains grow between Ti_3AlC_2 structures, and (iv) the TiC particles grow due to an insufficient amount of Al atoms for MAX phase formation (Figure 5C). When the process is finished, the polycrystalline Ti_3AlC_2 sinter is obtained (Figure 5D). The mortar grinding/ball milling treatments break the pellet structure, decrease the size of the particles and release $\alpha\text{-Al}_2\text{O}_3$ and TiC impurities. Part of the ingrown alumina particles remain embedded in the Ti_3AlC_2 matrix (Figure 5E). The aluminum atoms are removed from the MAX phase by hydrofluoric acid treatment, which lead to the formation of the multilayered MXene structure. The HF acid has no influence onto TiC or $\alpha\text{-Al}_2\text{O}_3$ particles, thus they are present as an impurity in the $\text{Ti}_3\text{C}_2\text{T}_x$ sample (Figure 5F).

4. Conclusions

We investigated and explained the influence of oxygen concentration during MAX phase preparation on the formation of alumina particles during MAX phase sintering, and thus on the properties of derived MXenes. High concentrations of O_2 molecules adsorbed on $\text{TiC}/\text{Ti}_2\text{AlC}$ particles or inside the cold-pressed pellet led to the increased formation of $\alpha\text{-Al}_2\text{O}_3$ particles in the Ti_3AlC_2 matrix. The hydrofluoric acid treatment led to the formation of multilayered $\text{Ti}_3\text{C}_2\text{T}_x$ featured by the presence of ingrown alumina particles and a plethora of structural holes created after the particles fell out. $\text{Ti}_3\text{C}_2\text{T}_x$ obtained by the conditioning of $\text{TiC-Ti}_2\text{AlC}$ powders in an O_2 environment possessed two-fold lower specific surface area in comparison with MXenes obtained by the conditioning of powders mixture in the Ar -filled glovebox. Therefore, in order to prepare high quality MXenes, oxygen should be avoided at each step of preparation—starting from weighing of the powders for Ti_3AlC_2 sintering and going all the way to the removal of O_2 molecules adsorbed on the MAX phase pellet surface before sintering.

The presence of large holes in the $\text{Ti}_3\text{C}_2\text{T}_x$ structure brings an opportunity to fill them with i.e., magnetic or catalytically active particles, or bioactive molecules, which could broaden potential application of multilayered MXenes toward environmental remediation, catalysis or drug delivery systems. The only issue is the plethora of remaining $\alpha\text{-Al}_2\text{O}_3$ impurities, which are hard to remove due to the natural resistance to wet chemistry methods and emplacement in the MXene structure. We believe that applying intercalation/delamination procedures could lead to the formation of tiny, hydrophilic $\text{Ti}_3\text{C}_2\text{T}_x$ monolayers due to the already fragmented multilayered structure. Then, as-prepared MXenes could be separated from the insoluble $\alpha\text{-Al}_2\text{O}_3$ particles by several simple washing-centrifugation cycles.

Currently, all experimental approaches related to preparation of tiny monolayers are based on: (i) extensive mechanical grinding and ball milling of the MAX phases, or (ii) ultrasound treatment of the multilayer MXenes, to delaminate and cut MXene layers into pieces. The former approach can result in severe damage to the MXene flakes after the etching process, and later can lead to the formation of structural defects and MXene decomposition. Actually, we believe that the preparation of multilayered MXenes with a plethora of structural holes could be a novel approach and also an efficient route for obtaining small MXene monolayers without the risk of defects formation or decomposition of the structure.

Supplementary Materials: The following are available online at <http://www.mdpi.com/1996-1944/12/3/353/s1>. Figure S1—The SEM micrographs (A–E) and EDS analysis (F) of the Al_2O_3 layer scratched from the Ti_3AlC_2 pellets and deposited on the carbon tape. Figure S2—The SEM micrographs of $\text{Ti}_3\text{AlC}_2\text{-Air}$ (A,C) and $\text{Ti}_3\text{AlC}_2\text{-Ar}$ (B,D), lightly broken pellets presenting triangle-shaped $\alpha\text{-Al}_2\text{O}_3$ nanoparticles (C) and highly symmetrical leftover holes (D).

Author Contributions: B.S. coordinated the research, carried out the preparation of the Ti_3AlC_2 , the formation of the MXenes and the XRD patterns analyses; V.K. investigated the SSA and porosity of MXene and MAX powders via physisorption analysis; B.P. characterized the sample morphology by SEM; M.J. performed the powder XRD measurements; K.T. contributed to the discussion of porosity measurements.

Funding: This work was financially supported by the National Science Centre of Poland SONATA Program, 2015–2018, grant No. 2014/13/D/ST5/02824 and SONATA Program, 2017–2019, grant No. 2016/21/D/ST3/00975.

Acknowledgments: The authors wish to acknowledge the technical assistance provided by P. Florczak.

Conflicts of Interest: The authors declare no conflicts of interest.

References

1. Novoselov, K.S.; Geim, A.K.; Morozov, S.V.; Jiang, D.; Zhang, Y.; Dubonos, S.V.; Grigorieva, I.V.; Firsov, A.A. Electric Field Effect in Atomically Thin Carbon Films. *Science* **2004**, *306*, 666–669. [[CrossRef](#)]
2. Anasori, B.; Lukatskaya, M.R.; Gogotsi, Y. 2D metal carbides and nitrides (MXenes) for energy storage. *Nat. Rev. Mater.* **2017**, *2*, 1–17. [[CrossRef](#)]
3. Lukatskaya, M.R.; Mashtalir, O.; Ren, C.E.; Dall’Agnese, Y.; Rozier, P.; Taberna, P.L.; Naguib, M.; Simon, P.; Barsoum, M.W.; Gogotsi, Y. Cation Intercalation and High Volumetric Capacitance of Two-Dimensional Titanium Carbide. *Science* **2013**, *341*, 1502–1505. [[CrossRef](#)]
4. Barsoum, M.W. *MAX Phases: Properties of Machinable Ternary Carbides and Nitrides*, 1st ed.; Wiley-VCH Verlag GmbH & Co. KGaA: Berlin, Germany, 2013; ISBN 978-3-527-33011-9.
5. Hu, M.; Hu, T.; Li, Z.; Yang, Y.; Cheng, R.; Yang, J.; Cui, C.; Wang, X. Surface Functional Groups and Interlayer Water Determine the Electrochemical Capacitance of $\text{Ti}_3\text{C}_2\text{T}_x$ MXene. *ACS Nano* **2018**, *12*, 3578–3586. [[CrossRef](#)] [[PubMed](#)]
6. Naguib, M.; Kurtoglu, M.; Presser, V.; Lu, J.; Niu, J.; Heon, M.; Hultman, L.; Gogotsi, Y.; Barsoum, M.W. Two-Dimensional Nanocrystals Produced by Exfoliation of Ti_3AlC_2 . *Adv. Mater.* **2011**, *23*, 4248–4253. [[CrossRef](#)]
7. Dall’Agnese, Y.; Lukatskaya, M.R.; Cook, K.M.; Taberna, P.-L.; Gogotsi, Y.; Simon, P. High capacitance of surface-modified 2D titanium carbide in acidic electrolyte. *Electrochem. Commun.* **2014**, *48*, 118–122. [[CrossRef](#)]

8. Natu, V.; Clites, M.; Pomerantseva, E.; Barsoum, M.W. Mesoporous MXene powders synthesized by acid induced crumpling and their use as Na-ion battery anodes. *Mater. Res. Lett.* **2018**, *6*, 230–235. [[CrossRef](#)]
9. Dong, Y.; Zheng, S.; Qin, J.; Zhao, X.; Shi, H.; Wang, X.; Chen, J.; Wu, Z.-S. All-MXene-Based Integrated Electrode Constructed by Ti_3C_2 Nanoribbon Framework Host and Nanosheet Interlayer for High-Energy-Density Li-S Batteries. *ACS Nano* **2018**, *12*, 2381–2388. [[CrossRef](#)] [[PubMed](#)]
10. Zhang, C.J.; Nicolosi, V. Graphene and MXene-based transparent conductive electrodes and supercapacitors. *Energy Storage Mater.* **2019**, *16*, 102–125. [[CrossRef](#)]
11. Zhang, Y.; Wang, L.; Zhang, N.; Zhou, Z. Adsorptive environmental applications of MXene nanomaterials: A review. *RSC Adv.* **2018**, *8*, 19895. [[CrossRef](#)]
12. Liu, J.; Liu, Y.; Xu, D.; Zhu, Y.; Peng, W.; Li, Y.; Zhang, F.; Fan, X. Hierarchical “nanoroll” like $\text{MoS}_2/\text{Ti}_3\text{C}_2\text{T}_x$ hybrid with high electrocatalytic hydrogen evolution activity. *Appl. Catal. B* **2019**, *241*, 89–94. [[CrossRef](#)]
13. Wen, Y.; Rufford, T.E.; Chen, X.; Li, N.; Lyu, M.; Dai, L.; Wang, L. Nitrogen-doped $\text{Ti}_3\text{C}_2\text{T}_x$ MXene electrodes for high-performance supercapacitors. *Nano Energy* **2017**, *38*, 368–376. [[CrossRef](#)]
14. Wang, Y.; Li, Y.; Qiu, Z.; Wu, X.; Zhou, P.; Zhou, T.; Zhao, J.; Miao, Z.; Zhou, J.; Zhuo, S. $\text{Fe}_3\text{O}_4@/\text{Ti}_3\text{C}_2$ MXene hybrids with ultrahigh volumetric capacity as an anode material for lithium-ion batteries. *J. Mater. Chem. A* **2018**, *6*, 11189–11197. [[CrossRef](#)]
15. Shen, C.; Wang, L.; Zhou, A.; Zhang, H.; Chen, Z.; Hu, Q.; Qin, G. MoS_2 -Decorated Ti_3C_2 MXene Nanosheet as Anode Material in Lithium-Ion Batteries. *J. Electrochem. Soc.* **2017**, *164*, 2654–2659. [[CrossRef](#)]
16. Tang, H.; Hu, Q.; Zheng, M.; Chi, Y.; Qin, X.; Pang, H.; Xu, Q. MXene–2D layered electrode materials for energy storage. *Prog. Nat. Sci. Mater. Int.* **2018**, *28*, 133–147. [[CrossRef](#)]
17. Ai, T.; Wang, F.; Zhang, Y.; Jiang, P.; Yuan, X. Synthesis and mechanism of ternary carbide Ti_3AlC_2 by in situ hot pressing process in TiC–Ti–Al system. *Adv. Appl. Ceram.* **2013**, *112*, 424–429. [[CrossRef](#)]
18. Rouquerol, J.; Rouquerol, F.; Llewellyn, P.; Maurin, G.; Sing, K. *Adsorption by Powders and Porous Solids*, 2nd ed.; Academic Press/Elsevier: Amsterdam, The Netherlands, 2014; ISBN 978-0-08-097035-6.
19. Sen, W.; Sun, H.; Yang, B.; Xu, B.; Ma, W.; Liu, D.; Dai, Y. Preparation of titanium carbide powders by carbothermal reduction of titania/charcoal at vacuum condition. *Int. J. Refract. Met. Hard Mater.* **2010**, *28*, 628–632. [[CrossRef](#)]
20. Melchior, S.; Raju, A.K.; Ike, I.S.; Erasmus, R.M.; Kabongo, G.; Sigalas, I.; Iyuke, S.E.; Ozoemena, K.I. High-voltage symmetric supercapacitor based on 2D titanium carbide (MXene, Ti_2CT_x)/carbon nanosphere composites in neutral aqueous electrolyte. *J. Electrochem. Soc.* **2018**, *165*, 501–511. [[CrossRef](#)]
21. Wang, S.; Ma, J.; Zhu, S.; Cheng, J.; Qiao, Z.; Yang, J.; Liu, W. High temperature tribological properties of Ti_3AlC_2 ceramic against SiC under different atmospheres. *Mater. Des.* **2015**, *67*, 188–196. [[CrossRef](#)]
22. Hu, L.; Benitez, R.; Basu, S.; Karaman, I.; Radovic, M. Processing and characterization of porous Ti_2AlC with controlled porosity and pore size. *Acta Mater.* **2012**, *60*, 6266–6277. [[CrossRef](#)]
23. Alhabeab, M.; Malesky, K.; Anasori, B.; Lelyukh, P.; Clark, L.; Sin, S.; Gogotsi, Y. Guidelines for Synthesis and Processing of Two-Dimensional Titanium Carbide ($\text{Ti}_3\text{C}_2\text{T}_x$ MXene). *Chem. Mater.* **2017**, *29*, 7633–7644. [[CrossRef](#)]
24. Syamsai, R.; Kollu, P.; Heong, S.K.; Grace, A.N. Synthesis and properties of 2D-titanium carbide MXene sheets towards electrochemical energy storage applications. *Ceram. Int.* **2017**, *43*, 13119–13126. [[CrossRef](#)]
25. Sadabadi, H.; Aftabtalab, A.; Zafaria, S.; Shaker, S.; Ahmadipour, M.; Venkateswara Rao, K. High purity Alpha Alumina nanoparticle: Synthesis and characterization. *IJSER* **2013**, *4*, 1593–1596.
26. Prikhna, T.; Ostash, O.; Sverdun, V.; Karpest, M.; Zimych, T.; Ivasyshin, A.; Cabioc’h, T.; Chartier, P.; Dub, S.; Javorska, L.; et al. Presence of Oxygen in Ti–Al–C MAX Phases-Based Materials and their Stability in Oxidizing Environment at Elevated Temperatures. *Acta Phys. Pol. A* **2018**, *133*, 789–793. [[CrossRef](#)]
27. Kruk, M.; Jaroniec, M. Gas Adsorption Characterization of Ordered Organic–Inorganic Nanocomposite Materials. *Chem. Mater.* **2001**, *13*, 3169–3183. [[CrossRef](#)]
28. Peng, C.; Wei, P.; Chen, X.; Zhang, Y.; Zhu, F.; Cao, Y.; Wang, H.; Yu, H.; Peng, F. A hydrothermal etching route to synthesis of 2D MXene (Ti_3C_2 , Nb_2C): Enhanced exfoliation and improved adsorption performance. *Ceram. Int.* **2018**, *44*, 18886–18893. [[CrossRef](#)]
29. Ahmed, B.; Anjum, D.H.; Hedhili, M.N.; Gogotsi, Y.; Alshareef, H.N. H_2O_2 assisted room temperature oxidation of Ti_2C MXene for Li-ion battery anodes. *Nanoscale* **2016**, *8*, 7580–7587. [[CrossRef](#)]
30. Li, J.; Yuan, X.; Lin, C.; Yang, Y.; Xu, L.; Du, X.; Xie, J.; Lin, J.; Sun, J. Achieving High Pseudocapacitance of 2D Titanium Carbide (MXene) by Cation Intercalation and Surface Modification. *Adv. Energy Mater.* **2017**, *7*, 160272. [[CrossRef](#)]

31. Wang, H.; Zhang, J.; Wu, Y.; Huang, H.; Jiang, Q. Chemically functionalized two-dimensional titanium carbide MXene by in situ grafting-intercalating with diazonium ions to enhance supercapacitive performance. *J. Phys. Chem. Solids* **2018**, *115*, 172–179. [[CrossRef](#)]
32. Li, Z.; Zhuang, Z.; Lv, F.; Zhu, H.; Zhou, L.; Luo, M.; Zhu, J.; Lang, Z.; Feng, S.; Chen, W.; et al. The Marriage of the FeN₄ Moiety and MXene Boosts Oxygen Reduction Catalysis: Fe 3d Electron Delocalization Matters. *Adv. Mater.* **2018**, *30*, 1803220. [[CrossRef](#)]



© 2019 by the authors. Licensee MDPI, Basel, Switzerland. This article is an open access article distributed under the terms and conditions of the Creative Commons Attribution (CC BY) license (<http://creativecommons.org/licenses/by/4.0/>).